Journal of Biomedical Optics

SPIEDigitalLibrary.org/jbo

Spectroscopic sensitive polarimeter for biomedical applications

Jessica C. Ramella-Roman
Amritha Nayak
Scott A. Prahl

Spectroscopic sensitive polarimeter for biomedical applications

Jessica C. Ramella-Roman,[a] Amritha Nayak,[b] and Scott A. Prahl[c]
[a]The Catholic University of America, Biomedical Engineering Department, Michigan Avenue NE, Washington, DC 20064
[b]Eunice Kennedy Shriver National Institute of Child Health and Human Development, NICHD-NICHD, Bethesda, Maryland 20817
[c]Oregon Medical Laser Center, Providence St. Vincent Medical Center, 9205 SW Barnes Road, Portland, Oregon 97225

Abstract. We present the design and calibration of a spectroscopic sensitive polarimeter. The polarimeter can measure the full Stokes vector in the wavelength range 550 to 750 nm with 1-nm resolution and consists of a fiber-based spectrophotometer, a white light emitting diode light source, two liquid crystal retarders, and one polarizer. Calibration of the system is achieved with a scheme that does not require knowledge of the polarizing elements' orientation or retardation. Six intensity spectra are required to calculate the full spectrum Stokes vector. Error in the polarimeter is less than 5%. We report the Stokes vectors for light transmitted through nonscattering polarizing elements as well as a measurement of the depolarizing properties of chicken muscle at several wavelengths. [DOI: 10.1117/1.3561907]

Keywords: Stokes vector; spectroscopic polarimeter; Mueller matrix.

Paper 09523R received Nov. 23, 2009; revised manuscript received Jan. 12, 2011; accepted for publication Feb. 14, 2011; published online Apr. 13, 2011.

1 Introduction

Stokes vectors polarimeters have been used for many different applications, including assessment of surface roughness and subsurface structure,[1] remote sensing,[2] diagnosis of malignancy,[3] and characterization of cell and nuclei size and index of refraction,[4,5] to name a few applications. Fiber-based systems are usually limited to the collection of the first three terms of the Stokes vector, or the co- and cross-polarized components of the backscattered field.[5,6] This is due, in part, to space constraints but one important limiting factor in multispectral polarimeters is the wavelength dependence of some of its elements. In fact, most common wave-plates have wavelength-dependent retardation ability. To overcome this issue, calibration schemes have been used where the changes in retardation are accounted by using a calibration matrix. When using liquid crystal retarders (LCRs) this step corresponds to a matrix of voltage setting per wavelength to achieve identical retardation.[7]

In this paper, we present a new spectral polarimeter and a simple calibration mechanism that eliminates the spectral dependency of its elements. Our polarimeter is fiber-based and was used to calculate the Stokes vector of light transmitted through biological samples. The calibration in this paper makes no assumption about the orientation and retardation of its elements, and is based on an achromatic wave-plate and a rotating polarizer. Following a calibration step, only six measurements are necessary to produce a Stokes vector at all wavelengths.

Address all correspondence to Jessica Ramella-Roman, The Catholic University of America, Biomedical Engineering Department, 620 Michigan Avenue NE, Washington, DC 20064. Tel: 202 319 6247; Fax: 202 319 6247; E-mail: ramella@cua.edu.

2 Material and Methods

The spectroscopic Stokes polarimeter requires two main assemblies, a calibration assembly that is used once and a permanent measuring assembly used to construct the spectroscopic sensitive Stokes vectors. Components common to both setups are two liquid crystal retarders (LCR1 and LCR2) (Meadowlark Optics, Frederick, Colorado), a dichroic polarizer (P) whose orientation is parallel to the optical table (Fig. 1), a white light source, and a fiber-based spectrophotometer. Both LCRs are positioned at fixed angles (0 and 45 deg) with respect to P. The light source is a white light emitting diode (LED) (Advanced Illumination, Rochester, Vermont). Light from the LED is collimated using a plano-concave lens ($F = 10$ mm, Newport, Irvine, California) and an iris (Newport, Irvine, California), and the beam size is 2 mm in diameter. Light passing through the LCRs and the polarizer is collected by a fiber-based spectrophotometer (Ocean Optics, Dunedin, Florida) through a 600-μm multimode fiber connected to a fiber collimator. The LCRs and the spectrophotometer are controlled via serial communication with custom-made software (MATLAB, Mathworks, Natick, Massachusetts) running on a desktop computer (Dell, Austin, Texas); for each position of the LCRs, one spectrum is acquired.

The calibration of the system is achieved with a method developed originally by Boulbry et al.[8] Their system captured Stokes vector images at three different wavelengths but each wavelength measurement required a different set of voltages controlling the LCRs. Here we extend their methodology to more than 200 wavelengths and a unique set of measuring conditions; this allows for a simpler calibration and faster measurement. The calibration step requires the addition of two more elements in the assembly (Fig. 1, dashed boxes), a linear

1083-3668/2011/16(4)/047001/7/$25.00 © 2011 SPIE

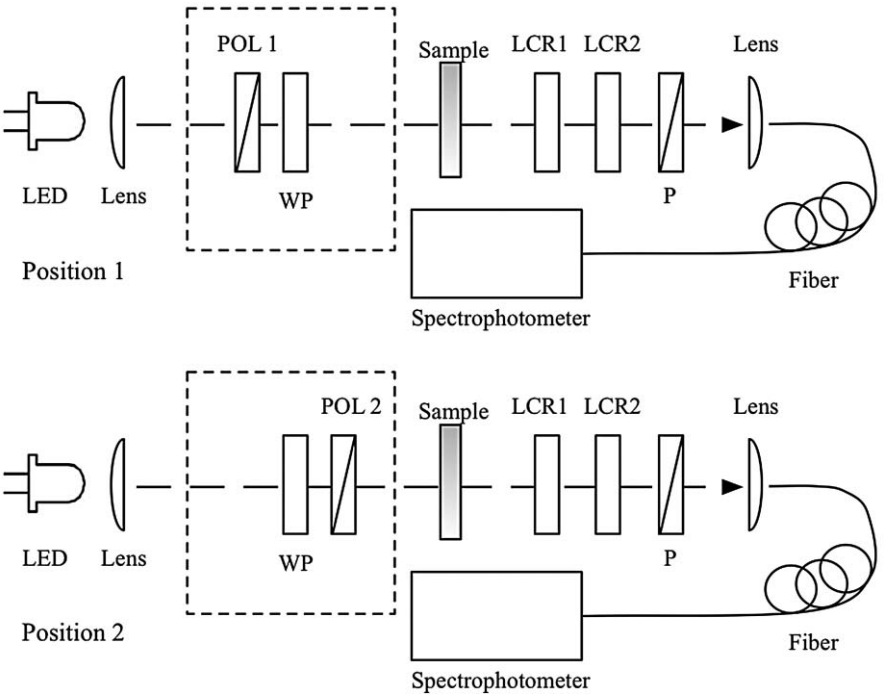

Fig. 1 Experimental layout. Position 1 and position 2 schematics refer to two different positions of the rotating polarizer.

polarizer (Melles Griot, Albuquerque, New Mexico) mounted on a motorized rotational stage (Thorlabs, Newton, New Jersey), and an achromatic wave-plate (Edmund Optics, Barrington, New Jersey).

The rotating polarizer is controlled through a desktop computer using MATLAB (Mathworks, Natick, Massachusetts), and is rotated in steps of 10° between a starting position at 0° and a final position at 180° to the collector polarizer. For each polarizer position, six full spectra are acquired by changing the retardation (δ_1 and δ_2) of the LCRs. This is accomplished by delivering six different voltage pairs to the LCRs. The voltage pairs are based on studies on the condition number of the reduction matrix W by Boulbry et al.[8] as well as their relation to the available wavelengths. We want to point out that a fixed set of voltages was used for all the wavelengths of interest, unlike what was previously proposed, with voltages that produced a fixed retardation at each wavelength. The six voltage pairs in this study were (V_1,V_2) = (5,5),(5,2),(3.8,2.8),(3.8,3.8),(5,3.8),(5,2.8), lower voltages are generally associated with higher retardation. In this way, a total of 19 × 6 spectra I_i are acquired for position 1 and position 2. A smaller interval polarizer orientation could be used to generate the calibration matrix and increase accuracy; nevertheless we found that 2 × 19 × 6 measurements yielded less than a 5% error.

Finally, 38 ideal calibration Stokes vectors are generated using an ideal set of polarizing elements using Eq. (1)

$$
\begin{aligned}
S_{\text{Calibration\_}i=0\ldots18} &= M_{\text{wavep}} M_{\text{pol}} S_{\text{unp}},\\
S_{\text{Calibration\_}i=0\ldots18} &= \begin{bmatrix} 1 & 0 & 0 & 0\\ 0 & 1 & 0 & 0\\ 0 & 0 & 0 & 1\\ 0 & 0 & -1 & 0 \end{bmatrix} \begin{bmatrix} 0.5 & \cos(2\theta) & \sin(2\theta) & 0\\ \cos(2\theta) & \cos(2\theta)^2 & \cos(2\theta)\sin(2\theta) & 0\\ \sin(2\theta) & \cos(2\theta)\sin(2\theta) & \sin(2\theta)^2 & 0\\ 0 & 0 & 0 & 0 \end{bmatrix} \begin{bmatrix} 1\\0\\0\\0 \end{bmatrix},\\
S_{\text{Calibration\_}i=19\ldots38} &= M_{\text{pol}} M_{\text{wavep}} S_{\text{unp}},\\
S_{\text{Calibration\_}i=19\ldots38} &= \begin{bmatrix} 0.5 & \cos(2\theta) & \sin(2\theta) & 0\\ \cos(2\theta) & \cos(2\theta)^2 & \cos(2\theta)\sin(2\theta) & 0\\ \sin(2\theta) & \cos(2\theta)\sin(2\theta) & \sin(2\theta)^2 & 0\\ 0 & 0 & 0 & 0 \end{bmatrix} \begin{bmatrix} 1 & 0 & 0 & 0\\ 0 & 1 & 0 & 0\\ 0 & 0 & 0 & 1\\ 0 & 0 & -1 & 0 \end{bmatrix} \begin{bmatrix} 1\\0\\0\\0 \end{bmatrix}.
\end{aligned}
\tag{1}
$$

The first equation, an unpolarized beam of light, is transmitted through an ideal polarizer with Mueller matrix M_{pol} at different orientations θ, and a wave-plate with fast axis parallel to the plane defined by the optical bench, with Mueller matix M_{wavep}. The second equation represents a similar layout where the positions of the polarizer and the wave-plate have been reversed.

The Stokes vectors generated using the above equations are related to the measured values I_i through the data reduction matrix W for which

$$S_i(\lambda) = W(\lambda)\, I_i(\lambda). \tag{2}$$

The data reduction matrix can be calculated as $W(\lambda) = S(\lambda)\ I_i(\lambda)^{-1}$ using the pseudo-inverse of I_i. Each $W(\lambda)$ is a 4×6 matrix. Random errors in the measurement can produce a number of nonzero singular values in the matrix I causing large errors in its pseudo-inverse. A truncated singular value decomposition of I is used to avoid this issue. Boulbry has shown that retaining only four singular values has only a minor impact on the resulting Stokes vectors. Finally, once $W(\lambda)$ is known, it can be used to calculate the Stokes vector spectrum for any measurement condition, regardless of sample or incident state of polarization. Ideal samples for this type of system are semi-transparent samples (low μ_a and low μ_s). Nevertheless, neither property compromises the system's ability to measure the transmitted Stokes vector as long as some transmitted light reaches the detector and is above the level of noise.[9]

3 Results

The ability of the system to produce correct Stokes vectors at each wavelength was tested by measuring light transmitted through known polarizing elements such as wave-plates and polarizers. Typical results are shown in Fig. 2. A linearly polarized incident state was generated by rotating a polarizer 90° with respect to the system reference plane (theoretical Stokes vector [1 –1 0 0]). An experimentally calculated Stokes vector for $\lambda = 600$ nm is shown below.

$$\mathrm{S}(600) = W(600)\, I(600)^T$$

$$\begin{bmatrix} 1.0186 \\ -1.0232 \\ 0.0089 \\ 0.0190 \end{bmatrix} = 10^{-4} \begin{bmatrix} 0.0554 & 0.0851 & 0.0025 & 0.1583 & 0.0168 & 0.1450 \\ 0.2705 & -0.2635 & 0.0662 & -0.0838 & 0.0523 & -0.0422 \\ 0.0102 & 0.0482 & 0.2402 & -0.3084 & 0.0454 & -0.0360 \\ 0.0348 & -0.0497 & -0.1068 & 0.0611 & -0.2605 & 0.3204 \end{bmatrix} \begin{bmatrix} 2173 \\ 39043 \\ 18368 \\ 20044 \\ 16803 \\ 22384 \end{bmatrix}^T. \tag{3}$$

In a second test, an incident circular polarized state was generated by combining a polarizer and a quarter-wave-plate (theoretical Stokes vector [1 0 0 1]). Experimental Stokes vectors obtained between 550 and 750 nm match theory and an experimental error of less than 5% at each wavelength is achieved as shown in the residuals graphs.

The system can also be used as a Mueller matrix polarimeter by changing the status of the incident polarization in four distinct ways as described by Rakovicet et al.[10] The average Mueller matrix of air between 550 and 750 nm was calculated and results are shown in the matrix below.

$$\sum_{k=550}^{750} M = \begin{bmatrix} 1.000 & 0.000 & 0.000 & 0.000 \\ 0.004 & 0.990 & -0.016 & 0.019 \\ 0.00 & 0.007 & 1.003 & 0.033 \\ 0.00 & -0.003 & -0.004 & 1.022 \end{bmatrix} \pm \begin{bmatrix} 0.000 & 0.000 & 0.000 & 0.000 \\ 0.008 & 0.011 & 0.013 & 0.019 \\ 0.016 & 0.019 & 0.037 & 0.035 \\ 0.010 & 0.010 & 0.023 & 0.029 \end{bmatrix}. \tag{4}$$

As expected, the Mueller matrix of air has values equal to 1 in the main diagonal and 0 otherwise. The errors associated with this measurement are reported in the matrix on the right as the standard deviation of the mean. Once again, the test shows that the system is capable of accurate reconstruction of polarimetric properties with errors below 5%.

Several authors, including this paper's, have shown that muscle tissue has polarizing properties.[11–14] However, to our knowledge, this has been demonstrated only at selected wavelengths. Figure 3 shows a map of the degree of polarization of light transmitted through a slab of chicken muscle at more than 200 wavelengths and 18 different orientations of the muscle bundles. In this experiment, freshly excised chicken breast tissue was placed on a rotational stage with the muscle bundles aligned parallel to the layout reference plane. Sample thickness was ~0.05 cm and light incident on the sample was po-

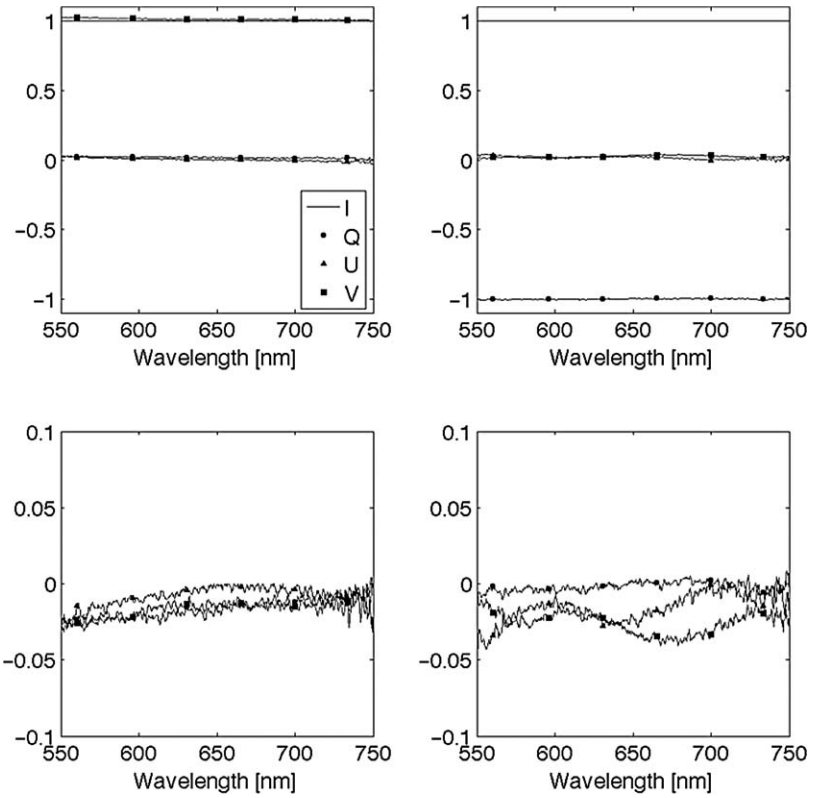

Fig. 2 Stokes vector results and residuals for incident circular polarized light (left) and linearly polarized light (90° orientation to the reference plane).

larized parallel to the reference plane. The sample was rotated in intervals of 10°. For each muscle position, a full-spectrum Stokes vector was obtained with our polarimeter and the degree of linear and degree of circular polarization was calculated.

Chicken muscle tissue behaves similarly to a quarter-wave retarder, as shown in the insert of Fig. 3, changing the status of the impinging polarized beam in a predictable manner. The insert graph was generated using an ideal Mueller matrix of a quarter-wave-plate ($\boldsymbol{M}_{\mathrm{dep}}$) at different orientation angles θ

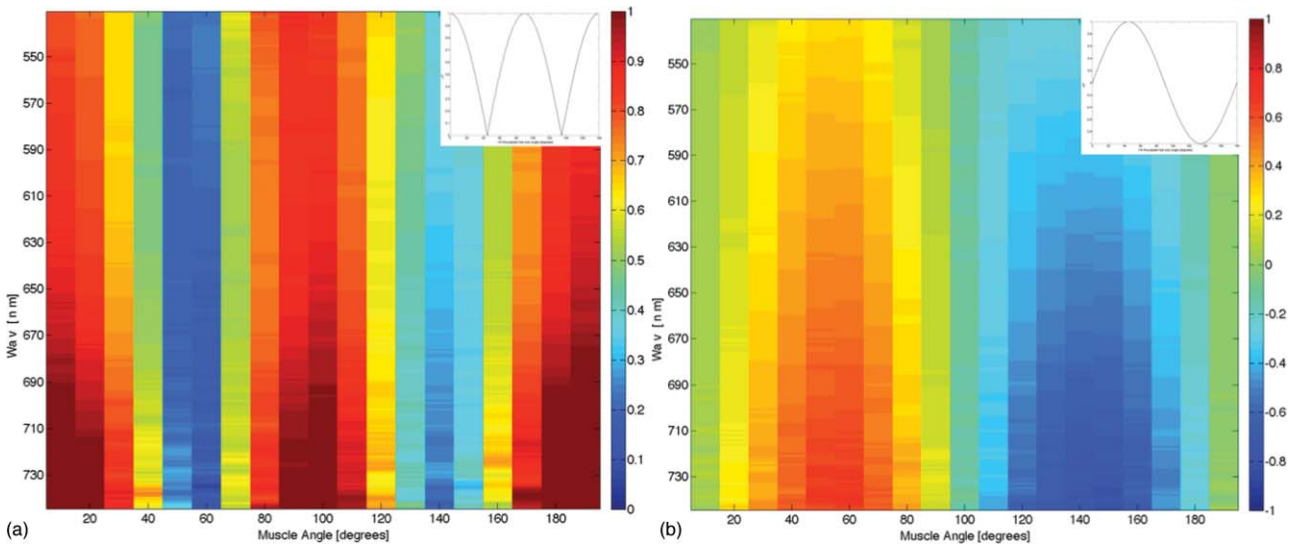

Fig. 3 Degree of linear polarization (a) for chicken muscle sample rotated at 18 different angles with respect to the reference plane. (b) The degree of circular polarization is reported. The inset shows the behavior of a polarizer–quarter-wave-plate combination where the quarter-wave-plate is rotated from 0 to 180°.

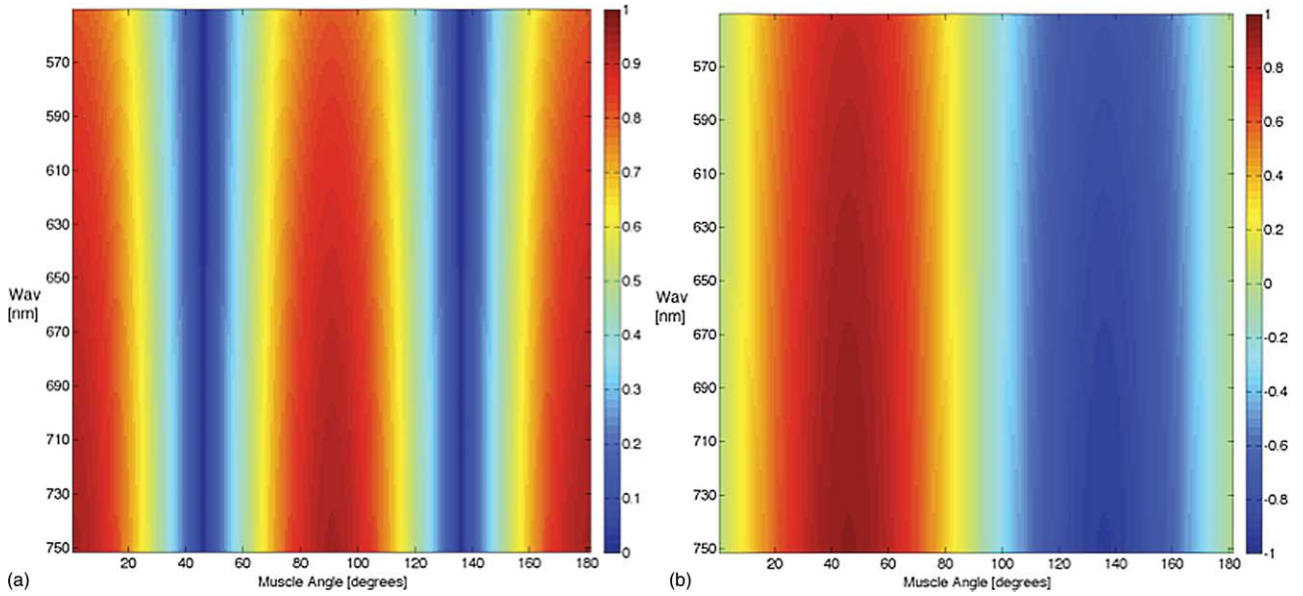

Fig. 4 Degree of linear polarization (a) for simulated chicken muscle sample rotated between 0 and 180° in 1° steps. Degree of circular polarization (b).

combined with a fixed polarizer oriented parallel to the main reference plane ($\boldsymbol{M}_{\text{pol}}$). The order of the theoretical optical train was source/polarizer/retarder/detector. The oscillatory pattern, maxima, and minima of the theoretical model are captured in the experimental data. Some wavelength dependence is noticeable in the experimental images, with longer wavelengths behaving more closely to the ideal model than shorter ones. This behavior can be explained if we consider the effect of the tissue microstructures scattering on the degree of polarization. Depolarization due to scattering is a well-known phenomenon[15,16] that can be represented with a Stokes diagonalizable Mueller matrix ($\boldsymbol{M}_{\text{dep}}$).

$$M_{\text{dep}} = \begin{bmatrix} 1.000 & 0.000 & 0.00 & 0.00 \\ 0.00 & [3(7/.10)^{n}]/[2+(7/10)^{n}] & 0.00 & 0.00 \\ 0.00 & 0.00 & [3(7/10)^{n}]/[2+(7/10)^{n}] & 0.00 \\ 0.00 & 0.00 & 0 & [3(1/2)^{n}]/[2+(7/10)^{n}] \end{bmatrix} \tag{5}$$

where $n+1$ is the number of scattering events.

As a first approximation, a predominant Rayleigh scattering was assumed for the chicken sample so that the behavior of light traveling through tissue could be simulated with the following optical train:

$$S_{\text{out}} = M_{\text{dep}}\, M_{\text{wav}}(\theta) M_{\text{pol}} S_i, \tag{6}$$

where S_i is the incident light Stokes vector and S_{out} is the resulting Stokes vector. Other authors have used a similar combination of small spherical scatterers (as an approximation of cellular organelles) and cylindrical silk fibers (simulating myofibrils constituting muscle fibers) to simulate polarized reflection from bulk muscle tissue.[17] Others have pointed out that depolarization in tissue is mainly affected by small scatterers.[18] Furthermore, scattering from cylinders is mostly in the direction perpendicular to the cylinder axis,[16] hence our approximation of a main depolarizing element as a Rayleigh aggregate is not unreasonable.

The wavelength dependence of scattering was captured using an expression of the form $\mu_{s'} = \text{A}\ \lambda^{-4}$, where λ is the wavelength of interest.[19] With this approximation, values of reduced scattering coefficient between 17 and 5 cm^{-1} in the range 550 to 750 nm were achieved; this particular range of optical properties was chosen to obtain a scattering coefficient of 9.6 cm^{-1} at 633 nm. Similar values at this wavelength have been reported by several authors.[19,20] Finally, the number of scattering events occurring in the 0.05-cm thick chicken slab is calculated for all 200 wavelengths and is an input to the Rayleigh scattering matrix. Results of the simulation are shown in Fig. 4.

The images in Fig. 4 capture the general behavior of the experiment conducted on chicken muscle. The reconstructed degree of linear polarization seems to agree more with its experimental counterpart than does the degree of circular polarization. In particular, experimental depolarization is greater than theoretical depolarization. This could be due to underestimating the reduced scattering coefficient $\mu_{s'}$ or it could be due to

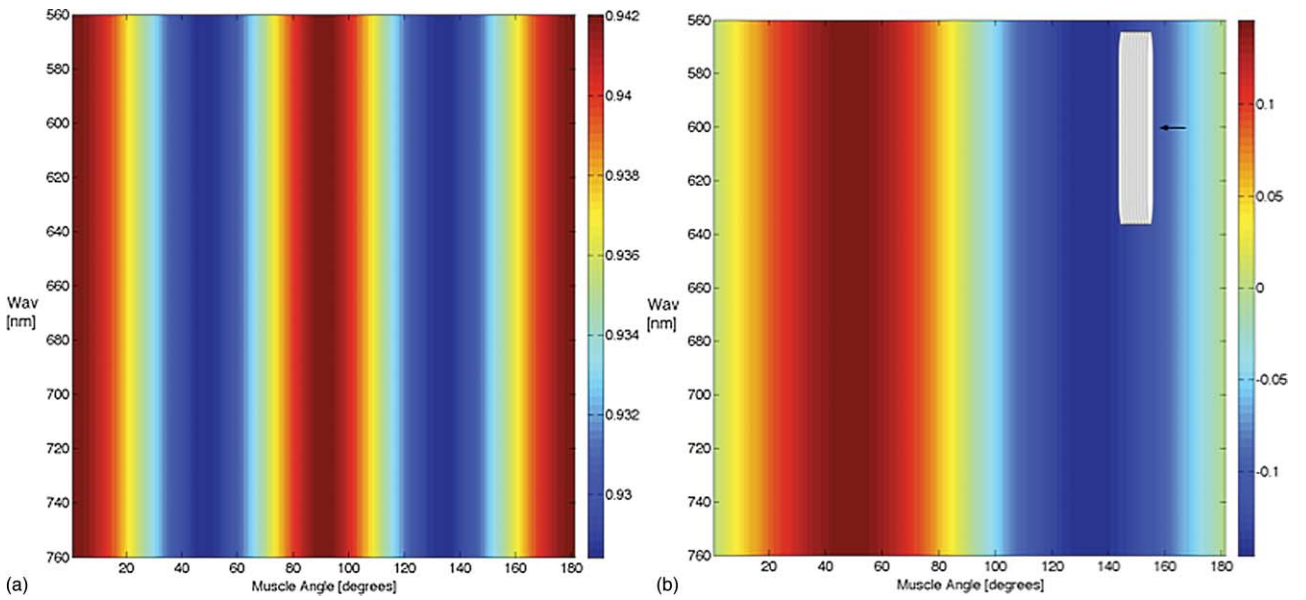

Fig. 5 Degree of linear polarization (a) and circular polarization (b) for simulated bundle of chicken muscle. A stack of 35 infinite cylinders (1.5-μm diameter), were used in this simulation. The incident beam was normal to the cylinder main axis with a Stokes vector equal to [1 1 0 0].

a nondiagonal depolarization.[21] Following the example of He et al.,[17] the Mueller matrix for muscle was also simulated as an infinite cylinder with an index of refraction of 1.4 surrounded by an environment with index of refraction of 1.33. A program originally developed by Bohren and Timbrell was used in all simulations.[15,22] The cylinder diameter was 1.5 μm and 35 cylinders were staked next to each other covering the slab length. A depolarizer was also added as described in Eq. (5). The oscillatory pattern of Figs. 3 and 4 are visible on the resulting images in Fig. 5, but resulted in a very small depolarization contrary to our experimental evidence. This may be attributable to inaccurate parameters for the density, size, and relative index of the cylindrical scatterers. The simulation is sensitive to relative index between the fibrils and their environment (which in our experiment is unknown). Finally, Mie theory assumes far-field interactions in the scattering field and this may be violated in the chicken muscle. Future work will focus on more realistic models of scattering from cylindrical structures in the near-field.

4 Conclusions

The Stokes vector polarimeter presented in this paper has a simple layout and requires only six measurements to achieve a full Stokes vector at 200 different wavelengths. Considering that the maximum time necessary to activate the liquid crystal retarders is on the order of 20 ms, a full spectrum Stokes vector could be captured in less than 200 ms, making this technique useful in the determination of spectro-polarimetric optical properties in tissue.

It is important to point out that the calibration procedure could be expanded to a larger range of wavelengths by using a broader spectrum light source and a Liquid Crystal Variable Retarder (LCVR) optimized for different regions of the spectrum (LCVRs tend to have fairly small working bandwidth) and multiple LCVR pairs may be necessary. Furthermore, the system could be modified to include imaging capability ultimately yielding a hyperspectral imaging Stokes vector system. This could be accomplished using either a liquid crystal tunable filter or filter wheel at the source and replacing the spectrophotometer with a camera. Such a system could be helpful in determining spatial changes in the polarimetric properties of tissue under different conditions.

Acknowledgments

We acknowledge and appreciate the financial support of the Applied Physics Laboratory, Johns Hopkins, Laurel, Maryland. Scott Prahl acknowledges the support of NIH/NIDCR 1R21DE016758.

References

1. T. A. Germer, C. Wolters, and D. Brayton, "Calibration of wafer surface inspection systems using spherical silica particles," *Opt. Express* **16**(7), 4698–4705 (2008).
2. G. Le Brun, B. Le Jeune, J. Cariou, and J. Lotrian, "Laser imaging procedure for evaluating the polarization signature of immersed targets," *Pure Appl. Opt.* **2**, 445–470 (1993).
3. K. Sokolov, L. T. Nieman, A. Myakov, and A. Gillenwater, "Polarized reflectance spectroscopy for pre- cancer detection," *Technol. Cancer Res. Treat.* **3**, 1–14, (2004).
4. J. R. Mourant, T. M. Johnson, and J. P. Freyer, "Characterizing mammalian cells and cell phantoms by polarized backscattering fiber-optic measurement," *Appl. Opt.* **40**(28), 5114–5123 (2001).
5. J. R. Mourant, T. M. Johnson, S. Carpenter, A. Guerra, T. Aida, and J. P. Freyer, "Polarized dependent spectroscopy of epithelial cells and epithelial cell nuclei to determine the size scale of scattering structures," *J. Biomed. Opt.* **7**, 378–387 (2002).
6. T. M. Johnson and J. R. Mourant, "Polarized wavelength-dependent measurements of turbid media," *Opt. Express* **4**(6), 200–216 (1999).
7. D. S. Kliger, J. W. Lewis, and C. E. Randall, *Polarized Light in Optics and Spectroscopy*, Academic Press, San Diego, CA (1990).

8. B. Boulbry, J. C. Ramella-Roman, and T. A. Germer, "Self-consistent calibration of a spectroellipsometer using a Fresnel rhomb as a reference sample," *Appl. Opt.* **46**, 8533–8541 (2007).
9. G. Zonios, "Noise and stray light characterization of a compact CCD spectrophotometer used in biomedical applications," *Appl. Opt.* **49**, 163–169 (2010).
10. M. J. Rakovic, G. W. Kattawar, M. Mehrubeoglu, B. D. Cameron, L. V. Wang, S. Rastegar, and G. L. Cote, "Light backscattering polarization patterns from turbid media: theory and experiment," *Appl. Opt.* **38**(15), 3399–3408 (1999).
11. J. C. Ramella-Roman and S. L. Jacques, "Mueller matrix description of collimated light transmission through liver, muscle and skin," in *Proc. SPIE* **4257**, 110–116 (2001).
12. B. H. Park, M. Pierce, B. Cense, and J. F. de Boer, "Jones matrix analysis for a polarization sensitive optical coherence tomography system using fiber optic components," *Opt. Lett.* **29**(21), 2512–2514 (2004).
13. S. L. Jacques, J. C. Ramella-Roman, and A. Moody, "Characterizing microscopic domains of birefringence in thin tissue sections," *Proc. SPIE* **4257**, 464–468 (2001).
14. V. Sankaran, J. T. Welsh, and D. Maitland, "Polarized light propagation through tissue phantoms containing densely packed scatterers," *Opt. Lett.* **25**(4), 239–241 (2000).
15. C. Brosseau, *Polarized Light–A Statistical Optics Approach*, John Wiley, New York (1998).
16. C. F. Bohren and D. Huffman, *Absorption and Scattering of Light by Small Particles*, John Wiley, New York (1983).
17. H. He, Z. Nan, L. Ran, Y. Tianliang, L. Wei, H. Yonghong, and M. Hui "Application of sphere-cylinder scattering model to skeletal muscle," *Opt. Express* **18**(14), 15104–15112 (2010).
18. N. Ghosh, M. F. G. Wood, S. Li, R. D. Weisel, B. C. Wilson, R. Li, and A. Vitkin, "Mueller matrix decomposition for polarized light assessment of biological tissues," *J. Biophotonics* **2**(3), 145–156 (2009).
19. B. C. Wilson, M. S. Patterson, and D. M. Burns, "Effect of photosensitiser concentration in tissue on the penetration depth of photoactivating light," *Lasers Med. Sci.* **1**, 235–244 (1986).
20. M. R. Arnfield, R. P. Mathew, J. Tulip, and M. S. McPhee, "Analysis of tissue optical coefficients using an approximate equation valid for comparable absorption and scattering," *Phys. Med. Biol.* **37**, 1219–1230 (1992).
21. R. Ossikovski, M. Foldyna, C. Fallet, and A. De Martino, "Experimental evidence for naturally occurring nondiagonal depolarizers," *Opt. Lett.* **34**, 2426–2428 (2009).
22. C. F. Bohren and V. Timbrell, "Computer programs for calculating scattering and absorption by normally illuminated infinite cylinders," Project No. 38, Institute of Occupational and Environmental Health, Montreal (1979).